SOME CHARACTERISTICS OF UPSIDE-DOWN STORMS IN THE NORTHERN SIERRA NEVADA, CALIFORNIA-NEVADA, USA

Benjamin J. Hatchett[1]*, Michael L. Kaplan[1] and Susan Burak[2]

[1]Desert Research Institute, Reno, NV, USA
[2]Snow Survey Associates, Bishop, CA, USA

ABSTRACT: Upside-down storms (UDSs) are winter precipitation events where temperature increases with time. We postulate that all mid-winter increases in streamflow will result from UDSs due to high snow levels and extreme precipitation. We identified UDSs using two 915 Mhz S-band snow level radars along the windward side of the northern Sierra Nevada and five streamflow gauges between 2010-2014. UDSs were defined as times when snow levels rose more than 500 m and took place during mid-winter increases in runoff. We explored the characteristics of these storms using atmospheric reanalysis products, surface weather and satellite observations. A prototypical case study is provided. With one exception, all UDSs coincided with mid-winter peak runoff events resulting from the high snow levels (mean snow level 2.2 km msl) and extreme precipitation (>95th percentile). All UDS cases occurred during the presence of one or more landfalling atmospheric rivers. The definition of UDSs should be expanded to include these key drivers of snow hydrological extremes (high snow levels, rain-on-snow, and extreme precipitation).

KEYWORDS: Upside-down storm, snow level, snow hydrology, atmospheric river.

1. INTRODUCTION

Winter precipitation events associated with rises in temperature are termed 'upside-down storms' (Atwater and Koziol, 1953; Atwater, 1954; hereafter UDSs). In lower elevation mountains such as the northern Sierra Nevada (Fig. 1) and the Washington Cascades, UDSs have important hydrometeorological impacts resulting from rain-on-snow and intense precipitation rates such as localized and large scale flooding (McCabe et al., 2007; Underwood et al., 2009; Neiman et al., 2011) and natural hazards such as debris flows (Carson, 2002). Rain-on-snow flooding disrupts montane stream ecosystems by favoring large sediment transport and changes in channel morphology but also contributes to habitat creation (Herbst and Cooper, 2010). In the Lake Tahoe Basin, where lake clarity is a concern, winter flooding events can wash large quantities of sediment and nutrients into the lake. UDSs pose problems for those concerned with commerce corridors such as Highways 50 and 80 (Fig. 1) as rapidly changing snow levels can substantially impact traffic restrictions and road closures. Lastly, UDSs create complex situations for water resource managers and dam operators who must balance minimizing flooding risks with maintaining reservoir storage for later warm season demands.

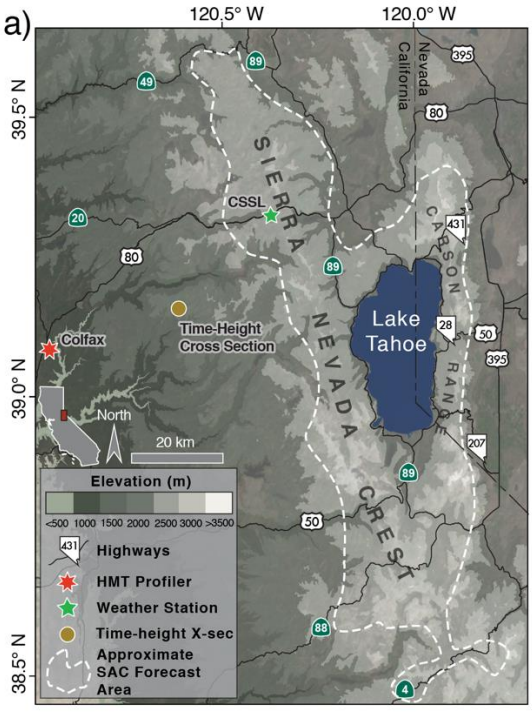

Fig. 1: Study area showing major roads, surface observations, cross section point, and Sierra Avalanche Center Forecast area.

Here, we objectively identify UDSs using a readily available surface-based remote sensing tool and

* *Corresponding author address:*
Benjamin J. Hatchett, Desert Research Institute, Reno, NV 89511;
tel: 775-674-7111;
email: benjamin.hatchett@dri.edu

observed river gauges in order to examine the atmospheric and hydrometeorological conditions associated with these events. We hypothesize that:

1) UDSs will be associated with all mid-winter peak streamflows.
2) UDSs will be associated with conditions of narrow, enhanced corridors of large horizontal moisture fluxes or atmospheric rivers (Zhu and Newell, 1998.
3) As a result of 2), extreme precipitation will be observed during UDSs.

2. DATA

Our study area is the northern Sierra Nevada of California and Nevada (Fig. 1) which is a moderate elevation (2000-3000 m), northwest-southeast trending midlatitude mountain range. Our study period spans November-March from 2010-2014. Hourly estimates of snow level were derived from the 915 Mhz S-band radar located at Colfax, CA (Fig. 1) and Sacramento, CA (~80 km southwest of Colfax; see Fig. 5). These radars are part of the National Oceanographic and Atmospheric Hydrometeorological Testbed (HMT) Profiler network (White et al., 2013). The data was provided by the Earth Systems Research Laboratory (http://www.esrl.noaa.gov). The snow level is estimated from the elevation of the radar bright band produced by strong reflectivity increases where melting and aggregation of hydrometeors occurs. This elevation is typically below the freezing level. Due to the greater number of snow level observations at Colfax compared to Sacramento (nearly double), we base our analysis on Colfax but also present results from Sacramento.

Archived Scanning Sensor Microwave Imagery (SSM/I; Schlüssel and Emery, 1990) estimates of precipitable water values over the northern Pacific Ocean were acquired from the University of Wisconsin (http:// tropic.ssec.wisc.edu/real-time/mimic-tpw/global/main.html).

Daily measurements of accumulated liquid precipitation at 21 Snowpack Telemetry (SNOTEL) stations were acquired from the National Resources Conservation Service website (http://www.nrcs.usda.gov; see Fig. 3). Hourly precipitation and 2 m temperature were acquired for the Central Sierra Snow Laboratory (CSSL) from the Western Regional Climate Center (http://www.wrcc.dri.edu). Daily forcing variables of liquid and frozen precipitation and model-simulated runoff from base of the snowpack at 1 km horizontal resolution were acquired from the Snow Data Assimilation System (SNODAS; NOHRSC 2004).

Atmospheric analysis at synoptic to meso-beta scales (150-2500 km) was performed with fields derived from the 3-hourly, 32 km horizontal resolution North American Regional Reanalysis (NARR; Mesinger et al., 2006). Archived daily Sierra Avalanche Center avalanche hazard forecasts were acquired for all UDSs from their website (http://www.sierraavalanchecenter.org). Streamflow for five rivers and streams were obtained from the United States Geological Survey's National Water Mapper (http://www.nwis.waterdata.usgs.gov). These gauges were selected because they capture key characteristic impacts of UDSs: flooding, water resources, habitat, and in the case of the Upper Truckee River, sediment and nutrient transport into Lake Tahoe.

3. METHODS

We defined an upside-down storm as an event when snow levels rose more than 500 m during a precipitation event or when snow levels were 500 m higher during the current precipitation event than the previous event. For the latter, we used a seven-day cutoff period. In all cases, we required at least six hours of radar data per event to avoid spurious snow level rises. All detected events were visually compared with raw data to ensure robustness. Of these events, we retained only those which occurred between Nov-Mar and also coincided with at least a doubling of streamflow from at least three gauges. We report the SAC avalanche hazard for these events.

To identify the presence of atmospheric rivers (ARs) in an Eulerian framework, we compared our dates to an AR catalog developed by Rutz et al., (2014). This catalog is based on NCEP/NCAR Reanalysis and uses integrated vapor transport (IVT) which exceeded 250 Kg m^{-1} s^{-1} and a length criteria of > 2000 km (Rutz et al., 2014) to identify ARs. We also calculated IVT from NARR products by vertically integrating the product of horizontal winds with specific humidity at each gridpoint.

NARR products were used to produce time-height cross sections at a point location upstream of the Sierra Crest (Fig. 1) for the layer spanning 800-150 hPa (e.g., Fig. 5). These types of cross sections are available as forecast products for many western North American mountain locations (e.g., http://www.weather.utah.edu) and can be generated for any point in global or regional forecast models. They assist in the identification of co-located moisture and instability on moist isentropic

surfaces, which can be used to evaluate the atmospheric layer's potential instability (resistance to cloud-scale buoyant vertical accelerations). The time-height cross sections were used to evaluate the vertical and temporal evolution of the atmosphere during two prototypical UDS case studies. NARR-derived upward vertical motion (omega, in Pa s^{-1}) is plotted to show simulated vertical motions that are favorable under saturated conditions. Moisture fluxes were calculated as the product of wind magnitude and specific humidity at each vertical level.

Precipitation intensity was estimated using SNOTEL data. We calculated the precipitation percentiles occurring during each event based upon all non-zero precipitation cool season days (Nov-Mar) spanning 1981-2014. To account for station reporting, the calculation took the maximum percentile met of the centered three-day window around each UDS event.

4. RESULTS

4.1 Radar and Streamflow-Identified Upside-Down Storm Events

Using the Colfax radar, we identified 14 dates (including three multi-day events) during which UDS conditions were satisfied. Upon selecting out events meeting the streamflow constraints, six events were retained: 18 Dec 2010, 14-16 Mar 2011, 20 Jan 2012, 14-16 Mar 2012, 30 Nov-2 Dec 2012, and 8-9 February 2014. These events are shown in Fig. 2 and highlighted in Fig. 4 with blue bars. Several cases (Fig. 2a, c, f) display classic UDS signals of rapidly rising snow levels. The 14-16 Mar 2011 and 2012 cases (Fig. 2b, d) demonstrate examples of a longer, slower warming trend. Summary statistics are provided in Fig. 3 for each radar. The mean snow level was 2.16 km (Colfax) and 2.38 km (Sacramento) above sea level. Sacramento has a higher mean value than Colfax (Fig. 3), which may suggest the presence of a strong horizontal temperature gradient becoming established during these storms. The 23-24 Oct 2010 event (green bar in Fig. 4) was associated with a typhoon that became entrained in the westerly flow and was transported across the Pacific. This event had high snow levels (>3500 m) but no pre-existing snowpack. Copious rainfall during this event produced significant streamflow increases and widespread flooding in California.

In the six UDS cases, substantial increases (up to an order of magnitude) in streamflow are evident for most if not all gauges shown in Fig. 4. All events had 'High' avalanche danger ratings and observed natural and human-triggered avalanches with the exception of the 14-16 Mar 2011 and 14-16 Mar 2012 periods, which had 'Considerable' ratings and widespread wet loose avalanches during the 2012 case.

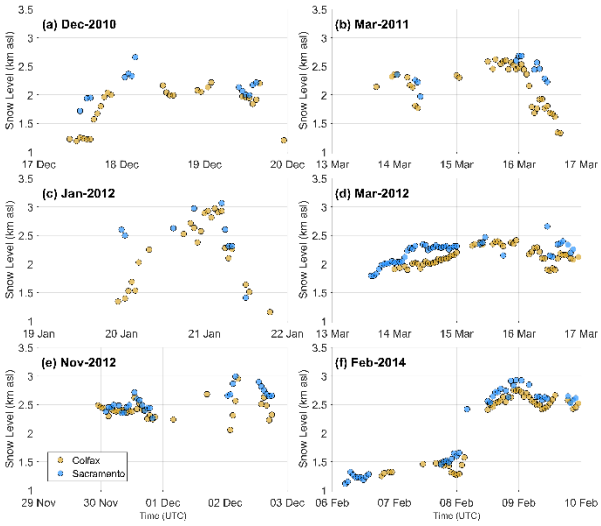

Fig. 2: (a-f) Brightband-derived estimates of snow level during the six individual upside-down storm events identified in the study using HMT radars.

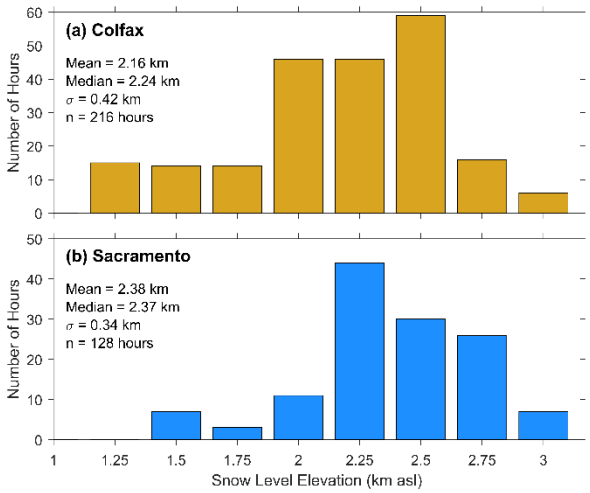

Fig. 3: Summary statistics for snow level radars spanning the period two days prior to upside-down storm events and one day after.

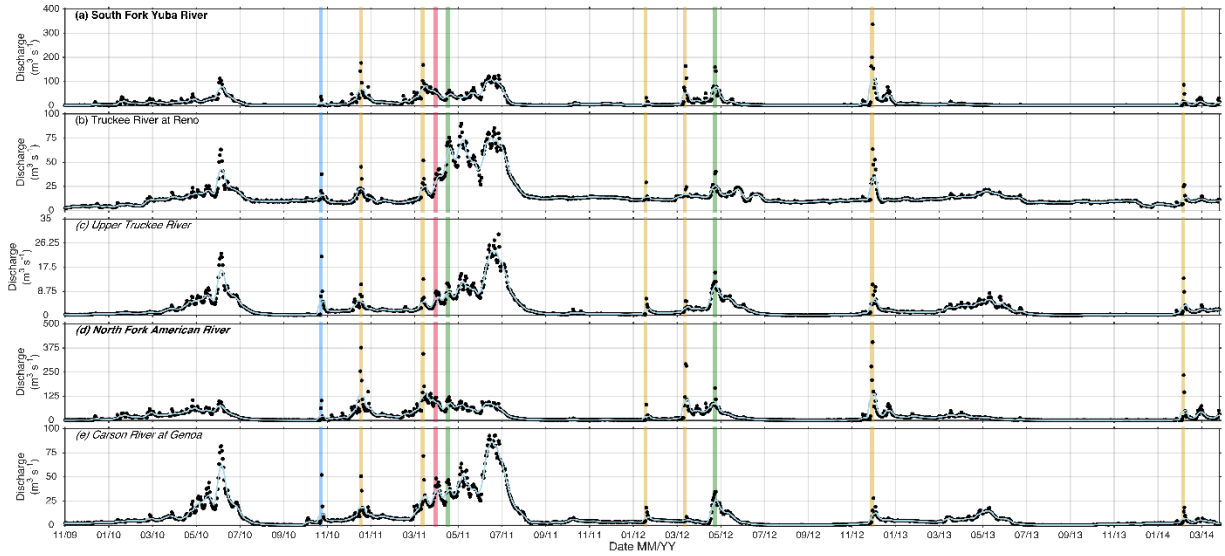

Fig. 4: Daily streamflow (discharge in $m^3 s^{-1}$) from five gauges in the northern Sierra Nevada. Dots are observations, thin blue lines are five-day running means. Unimpaired gauges have names italicized and bold gauges drain westward. Gold bars highlight periods identified by radar (Fig. 3) as having rises in snow level and by gauges as increases in streamflow. Green bars show late season (April) rain-on-snow events. The blue bar demonstrates when a typhoon made landfall and resulted in copious out-of-season precipitation. The red bar demonstrates an anomalous warming event. Gauge location is shown in Fig. 5.

4.2 *Precipitation During Upside-Down Storm Events*

The mean maximum precipitation percentile exceeded for all events and stations was 96, indicating the extreme nature of daily precipitation during the UDS events. Averaged over the six events, the range of mean percentiles exceeded by station spanned 93-98. These results are shown by shaded circles in Fig. 5. The highest values were well-distributed throughout the northern two-thirds of the study area, while the southern region, near Carson Pass and Hwy 88 (Fig. 1) showed lower overall values. This may be due to the fact that we used river gauges whose flow is favored by a more northerly storm track or by the more northerly location of the Colfax radar. Under such a storm track, stronger atmospheric convergence along the poleward side of the frontal system would lead to a large meridional precipitation gradient. Continuing work will seek to evaluate the origin of this finding, but nonetheless, extreme precipitation, as defined by daily values > 90th percentile, is a common attribute in UDS events. The high snow levels (2-2.75 km above sea level; Figs. 2-3) imply that a significant proportion of the northern Sierra Nevada watersheds are receiving heavy rainfall or rain-on-snow, which is consistent with the large increases in streamflow (Fig. 4).

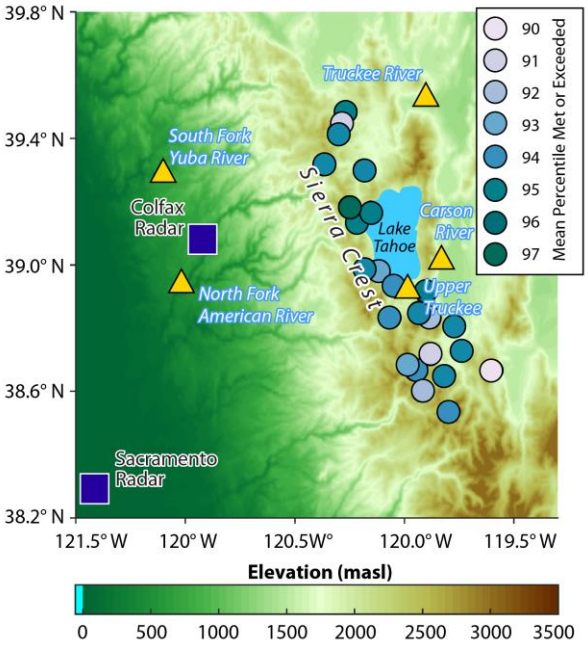

Fig. 5: SNOTEL stations (circles) are shaded by mean maximum precipitation percentile met or exceeded during UDSs.

4.3 *Case Study 1: 14-19 December 2010*

The 14-19 Dec 2010 storm cycle represents a quintessential UDS. The first storm which ended on 15 Dec 2010, underwent a cooling trend (right-

side up) with a 2000 m fall in snow level (Fig. 6a). During this first event, 80 mm of precipitation accumulated at CSSL and the moisture source was a modest plume of subtropical vapor entrained in the onshore zonal flow (Fig. 6b). On 17-19 Dec, a wetter (total observed precipitation of 110 mm between 17-18 Dec) and much warmer storm followed with snow levels that rose 1200 m during an 18-hour period (Fig. 6a). The SAC avalanche forecast rose to 'Extreme' on 18 Dec (Fig. 6a) amidst concerns for widespread instability due to much denser snow overlying less dense snow from the previous event. Similar to the first event, the warmer event had strong zonal moisture transport sourced from the same tropical moisture export west of Hawaii (Fig. 6c). Vertical cloud profiles (not shown) show ice phase clouds present up to 14 km and upstream of the Sierra Nevada. These clouds indicate deeper convection and strong vertical accelerations which contribute to intense precipitation, strong and gusty winds, and the formation of diverse crystal habits. Collectively, the presence of large scale ascent and favorable environment for strong vertical accelerations combined with a moisture source (the low-mid level AR) create ideal conditions for sustained heavy precipitation. The warm nature of this secondary wave produced widespread rain-on-snow leading to marked increases in streamflow on both sides of the Sierra Crest (Fig. 4).

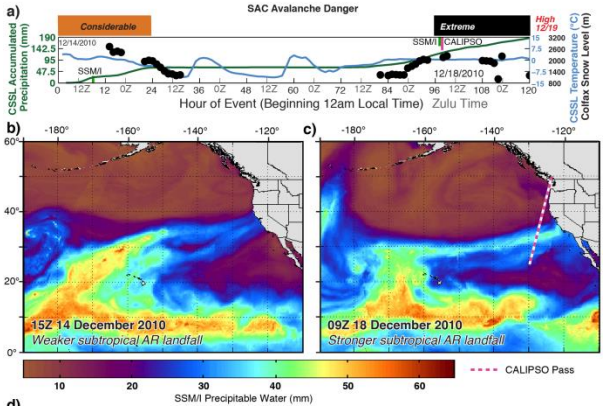

Fig. 6: (a) Station-based observations during the 15-19 Dec 2010 case study. (b-c) SSM/I-estimated precipitable water (mm) showing the landfalling atmospheric river.

Time-height cross sections (Fig. 7), which are read from right to left, show that the two storm events are characterized by mid-upper level (600-250 hPa) fronts and moist-neutral conditions (no change in saturated equivalent potential temperature with height). These conditions are conducive to positive buoyancy and correspond with shallow and deeper upward vertical motions (green-blue colors in Fig. 7a). During the second event, higher saturated equivalent potential temperatures are shown near the upstream mountain top height (700 hPa) and are indicative of a warmer airmass. The periods of moist-neutrality and upward vertical motions coincided with periods of enhanced moisture fluxes (Fig. 7b). While the first event had one primary moisture plume, the second event demonstrated three separate plumes of deep moisture. Strong upper level winds (70-85 m s^{-1}) and the establishment of deep, moist ascent to 300 hPa (Fig. 7) along with the low level moisture fluxes are consistent with the waves of intense precipitation during this event (Fig. 6a)

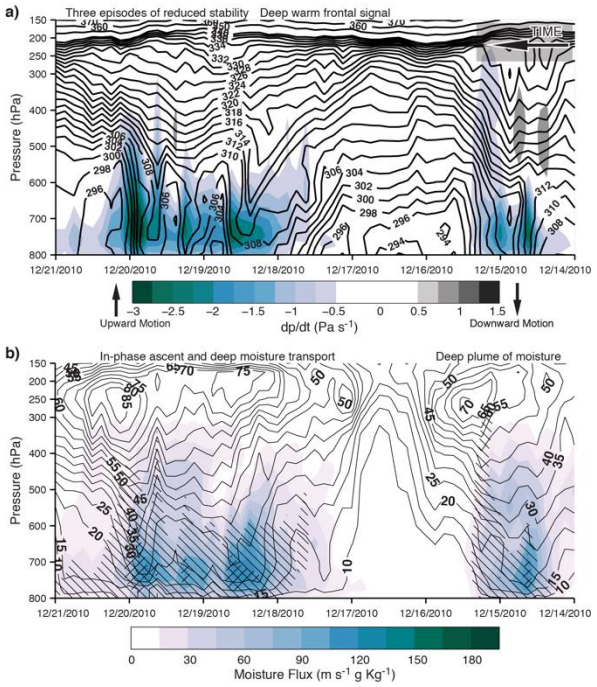

Fig 7: (a) Time-height cross section of saturated equivalent potential temperature (black contours, in Kelvin) and NARR-derived vertical motions (Pa s^{-1}) for the period 14-21 Dec 2010. (b) Similar to (a), with wind speeds (black contours, m s^{-1}), moisture flux (colors, m s^{-1} g Kg^{-1}), and hatches indicating upward vertical motions (single hatches for < -1 Pa s^{-1} and double for < -2 Pa s^{-1}).

A strong frontal boundary along the Sierra characterizes the second, warmer event at mid and low levels (Fig. 8c, e, g). At 775 hPa, 20 m s^{-1} southwesterly winds blow across the front, indicating strong warm air advection (Fig. 8c, e, g) that acts to increase snow levels and sustain precipitation. This warm air advection coincides with the landfalling moisture plume (AR) (Fig. 6c and 8d) and

dynamically contributes to mid-level warm frontogenesis and ascending vertical motions that further enhances precipitation rates. Topographic moisture convergence is evident along the Sierra (Fig. 8d, f, h) also leading to enhanced precipitation rates. A positively tilted upper level cyclone is present at 250 hPa (Fig. 8b, d, f, h). Consistent with warm advection, strong moisture flux convergence and sustained precipitation, the right anticyclonically sheared and diffluent exit region of the 250 hPa jet is over the Sierra Nevada for much of the period. Large-scale quasi-geostrophic upper level divergence is contributed by the curved exit region of this upper jet. A leeside trough can be inferred from the large geopotential height gradient along the Sierra Nevada (Fig. 8c, e, g).

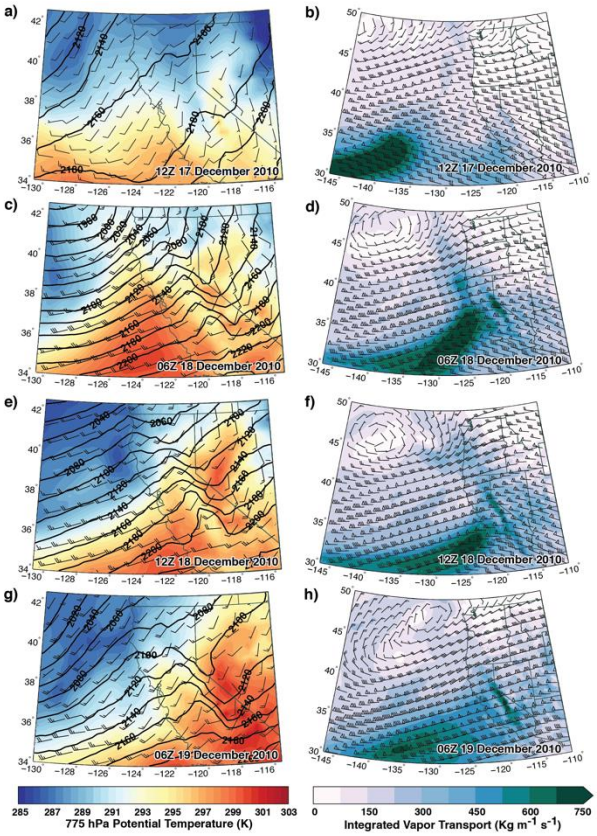

Fig. 8: (a,c,e,g) 775 hPa potential temperature (colors, in Kelvin), wind speeds (barbs, in m s^{-1}), and geopotential heights (black contours, m). (b,d,f,g) Integrated vapor transport (colors, Kg m^{-1} s^{-1}) and 250 hPa winds (barbs, in m s^{-1}). The period spanning 12Z 17 Dec-06Z 19 Dec is shown.

Spatial estimates of liquid and frozen precipitation during the period 17-20 Dec 2010 are shown in Fig. 9a-b. Much of the region received both forms of precipitation. Streamflow discharge increases as a result of snowmelt-derived runoff during this event, particularly along the western flank of the Sierra Nevada (Fig. 9c). Over 20 mm of rain-on-snow occurred along much of the Sierra Crest (Fig. 9a) leading to extreme avalanche hazard (Fig. 6a), but the crest did not contribute to snowmelt-derived runoff during this event (Fig. 9c).

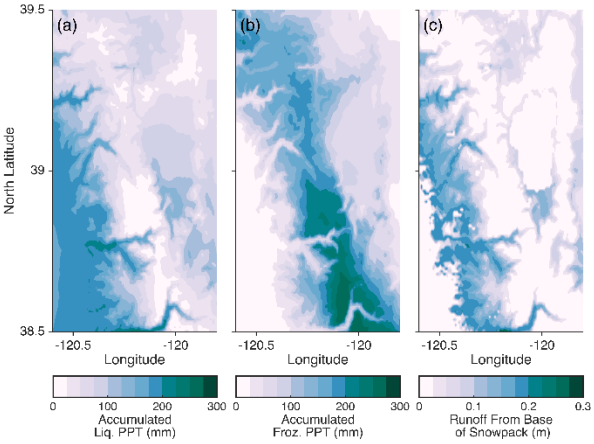

Fig. 9: SNODAS accumulated (a) liquid and (b) frozen precipitation and (c) runoff from the base of the snowpack over the period 17-20 Dec. The outline of Lake Tahoe is evident in (c).

4.4 *Atmospheric River Conditions During Upside-Down Storm Events*

All UDS events with rises in snow level and substantial increases in streamflow were associated with a landfalling atmospheric river when compared against the catalog of Rutz et al. (2014).

5. DISCUSSION AND CONCLUSIONS

Rises in snow levels that coincide with sustained, heavy to extreme precipitation produce a series of immediate challenges for weather and avalanche forecasters and reservoir operators. During these events, large increases in streamflow (Fig. 4) and subsequent flood hazard occur at the same time as impacts to travel along major transportation corridors that cross the Sierra Nevada. These events occur in tandem with considerable to extreme avalanche hazard. Bair (2013) has shown that positive air temperature trends did not help explain avalanche occurrence at Mammoth Mountain in the central Sierra but large changes in snow water equivalent was a better explanatory variable. In the lower elevation northern Sierra Nevada, the role of temperature may be enhanced due to the proximity to the rain-snow transition line. However, our findings that all UDSs are linked to AR landfall would lead us to believe that temperature

trends themselves are a much lower order contributor to avalanche occurrence. Separation of temperature and precipitation is difficult, but the extreme precipitation rates, strong winds, and the wide range of crystal habits formed by convective environments and associated microphysical processes (Minder and Kingsmill, 2013) during intense AR storms are likely the primary drivers of snowpack loading and increased avalanche activity. In other words, the temperature rises are a symptom of atmospheric processes related to AR landfall (heavy precipitation and high snow levels). Turbulent winds, intense precipitation and variety of crystal habits support formation of storm slabs and non-persistent weak layers.

The finding that all UDSs occur during AR conditions is not surprising but further demonstrates that ARs are key components of snow hydrological extremes in the northern Sierra Nevada. ARs are associated with nearly all mid-winter peak streamflow (Fig. 4) and many extreme precipitation (Fig. 5) events. These storms have high snow levels (Figs. 2-3) that favor the generation of runoff (Fig. 9c) via rain-on-snow and continued precipitation on lower elevation saturated soils. Such effects are pronounced if significant low elevation snow existed prior to the storm.

Warm air advection realized through positive temperature trends increases snow and freezing levels. Warm air advection also promotes upward vertical motions that favor intense precipitation rates (Fig. 9a, b) and subsequent snowpack loading (Fig. 5). However, other processes that offset warming or create snow level fluctuations during the storm may mask warming trends in surface-based observations (cf. Figs. 2 and 6a). These include upslope adiabatic cooling, evaporational cooling, and orographic precipitation enhancement; the latter contributes to latent cooling from melting of hydrometeors and allows frozen hydrometeors to descend below the freezing line (Minder et al., 2011).

Snow level radar provides a useful tool for observing rapid changes in snow level and forecasting subsequent impacts such as increases in runoff or travel restrictions. Snow level radar can be used to compare real-time observations and forecast snow levels to determine model forecast biases. Accurate forecasting of snow levels and the timing of snow level fluctuations can provide useful information to both operational weather and avalanche forecasters and emergency managers. Snow level radar can be used to find the optimal set of physics parameterization schemes in high resolution numerical weather models for environments near the rain-snow transition. Reducing forecast errors and uncertainty in snow levels during extreme precipitation events can better inform floodplain managers and reservoir operators on whether or not flooding is a major concern or if water can be stored (such as under otherwise persistent drought conditions). Rain-on-snow events are expected to increase in frequency under a warmer climate regime (McCabe et al., 2007) and montane systems at the present snow-rain transition are most likely to be affected by climate change (Herbst and Cooper, 2010). Ecohydrologic and geomorphological studies focused on evaluating projected changes in riparian and aquatic habitats can benefit from using observed snow levels to reduce biases from dynamically downscaled future climate output that serves as input to hydrologic or other impacts models (e.g., Mejia et al., 2012).

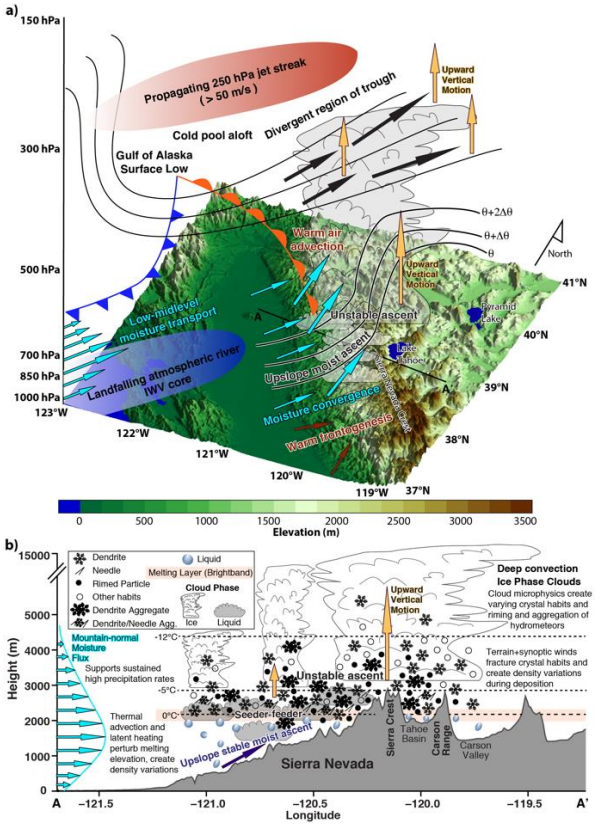

Fig. 9: (a) Oblique view of primary synoptic-mesoscale processes during upside-down storm events. (b) Cross section from west to east showing primary microphysical and mesoscale processes during upside-down storms that contribute to observed avalanche hazard and streamflow increases (note large fraction of the range lies beneath the melting layer).

In summary, we used observations and atmospheric reanalysis products to identify and evaluate upside-down storms. *All UDS events were associated with atmospheric rivers, had high snow levels (above 2 km), and extreme precipitation*, thus leading to 2-10 times increases in streamflow and rising avalanche hazard. The largest mid-winter season peak streamflow during the period studied (2010-2014) occurred during UDSs with one exception pertaining to an anomalous warm spell. Our results suggest that avalanche hazard resulting from upside-down storms is not the rising temperatures over the course of the storm but rather the conditions which tend to create this signal; notably, the presence of a concentrated plume of subtropical moisture, local moisture convergence, warm air advection, a strong front, deep convection, and strong winds. These same conditions directly contribute to flood and travel hazards. A summary of these processes is presented in a schematic (Fig. 9) with emphasis on the multiple scales and processes which lead to intense precipitation and subsequent runoff generation and snowpack instability.

The benefits of further studying UDSs lie primarily in understanding how to better forecast and simulate them for improved reservoir operation and to use them as future climate analogs for studies of ecohydrologic responses to a warming climate. The working definition of an upside-down storm in the avalanche vernacular should also be reconsidered to include the aforementioned important phenomena (notably ARs and extreme precipitation) which drive the avalanche hazard increases.

6. ADDITIONAL INFORMATION

CONFLICT OF INTEREST

The authors declare no conflicts of interest.

ACKNOWLEDGEMENTS

This work was supported by a Graduate Research Grant provided by the American Avalanche Association.

REFERENCES

Atwater, M.M., F.C. Koziol, 1953: *Avalanche Handbook*, 1st ed, 149.

Atwater, M.M., 1954: Snow avalanches, *Scientific America*, 190, 26-31.

Bair, E.H., 2013: Forecasting artificially-triggered avalanches in storm snow at a large ski area, *Cold Regions Science and Technology*, 85, 261-269.

Carson, R., 2002: Take the a-frame: debris flow during the 1996 rain-on-snow event, Blue Mountains, Washington. Proceedings of the *Geological Society of America Cordilleran Section Annual Meeting*, May 13-15, 2002.

Herbst, D.B. and S.D. Cooper, 2010: Before and after the deluge: rain-on-snow flooding effects on aquatic invertebrate communities of small streams in the Sierra Nevada, California. Journal of the North American Benthological Society, 29(4), 1354-1366.

McCabe, G.J., Clark, M.P., and L.E. Hay 2007 Rain-on-snow events in the western United States. *Bulletin of the American Meteorological Society*, 88, 319-328.

Mejia, J.F., Hatchett, B.J., Niswonger, R.,G., Huntington J.L., and D.K. Koracin. 2012: Linking global climate models to an integrated hydrologic model: Using an individual station downscaling approach. *Journal of Contemporary Water Research and Education*, 147, 17-27.

Mesinger, F. and Coauthors, 2006: North American Regional Reanalysis. *Bulletin of the American Meteorological Society*, 87, 343-360.

Minder, J.R., and D.E. Kingsmill, 2013: Mesoscale variations of the atmospheric snow line over the Northern Sierra Nevada: Multiyear statistics, case study, and mechanisms. *Journal of the Atmospheric Sciences*, 70, 916-938.

Minder, J.R., Durran, D.R., and D.E. Kingsmill, 2011: Mesoscale controls on the mountainside snowline. *Journal of the Atmospheric Sciences*, 68, 2107-2127.

Neiman, P. J, Schick, L.J., Ralph, F.M., Hughes, M., and G.A. Wick, 2011: Flooding in Western Washington: The connection to atmospheric rivers. *Journal of Hydrometeorology*, 12, 1337-1358.

National Operational Hydrologic Remote Sensing Center (NOHRSC), 2004: Snow data assimilation system (SNODAS) products at NSIDC, [2003-2016]. Boulder, Colorado, USA: National Snow and Ice Data Center (NSIDC). http://dx.doi.org/10.7265/N5TB14TC.

Osterhuber, R., and E. Kattelmann, 1998: Warm storms associated with avalanche hazard in the Sierra Nevada. Proceedings of the *International Snow Science Workshop*, 526-533.

Rutz, J.J., Steenburgh, W.J., and F.M. Ralph, 2014: Climatological characteristics of atmospheric rivers and their inland penetration over the western United States. *Monthly Weather Review*, 142, 905-921.

Schlüssel, P., and W.J. Emery, 1990: Atmospheric water vapour over oceans from SSM/I measurements. *International Journal of Remote Sensing*, 11, 753-766.

White, A.B., and Coauthors, 2013: A Twenty-first-century California observing network for monitoring extreme weather events. *Journal of Atmospheric and Oceanic Technology*, 30, 1585-1603.

Underwood, S.J., Kaplan, M.L., and K.C. King, 2009: The role of upstream midtropospheric circulations in the Sierra Nevada enabling leeside (spillover) precipitation. Part I: A synoptic-scale analysis of spillover precipitation and flooding in a leeside basin. *Journal of Hydrometeorology*, 10, 1309-1326.

Zhu, Y., and R.E. Newell, 1998: A proposed algorithm for moisture fluxes from atmospheric rivers. *Monthly Weather Review*, 126, 725-735.